Evaluating Motion Processing Algorithms for Use with Functional Near-infrared Spectroscopy Data from Young Children

Lourdes M. Delgado Reyes[1], Kevin Bohache[2], Sobanawartiny Wijeakumar[3], & John P. Spencer[1]

[1]School of Psychology, University of East Anglia, UK

[2]University of Iowa

[3]University of Stirling

Correspondence to:

John P. Spencer
School of Psychology
Room 0.09 Lawrence Stenhouse Building
University of East Anglia
Norwich Research Park
Norwich NR4 7TJ
United Kingdom

Email: j.spencer@uea.ac.uk

Accepted for publication in *Neurophotonics* published by SPIE.

Biographies

Lourdes Delgado Reyes is a PhD candidate in the School of Psychology at the University of East Anglia. She received an M.A. from the University of Iowa in 2015. Her research interest include understanding the neurobehavioral precursors of executive function in early development using a combination of fNIRS, MRI, and eye tracking methodologies.

Kevin Bohache received an M.A. from the University of Iowa in 2014. He is currently a high school science teacher at Teach for America in Cincinnati, OH.

Sobana Wijeakumar received her PhD in Visual Perception from Glasgow Caledonian University, Scotland, U.K. in 2012. She is a Lecturer in the School of Psychology at the University of Stirling, Scotland, U.K. Her research interests include understanding the neurobehavioral correlates of visual working memory, inhibition and cognitive flexibility along the lifespan using a combination of fNIRS, fMRI, EEG and eye-tracking methodologies.

John P. Spencer is a Professor of Psychology at the University of East Anglia in Norwich, UK. He received a Sc.B. with Honors from Brown University in 1991 and a Ph.D. in Experimental Psychology from Indiana University in 1998. He is the recipient of the 2003 Early Research Contributions Award from the Society for Research in Child Development, and the 2006 Robert L. Fantz Memorial Award from the American Psychological Foundation.

Corresponding Author: John P. Spencer, PhD

Abstract

Motion artifacts are often a significant component of the measured signal in functional near-infrared spectroscopy (fNIRS) experiments. A variety of methods have been proposed to address this issue, including principal component analyses (PCA), correlation-based signal improvement (CBSI), wavelet filtering, and spline interpolation. The efficacy of these techniques has been compared using simulated data; however, our understanding of how these techniques fare when dealing with task-based cognitive data is limited. Brigadoi et al. (2014) compared motion correction techniques in a sample of adult data measured during a simple cognitive task. Wavelet filtering showed the most promise as an optimal technique for motion correction. Given that fNIRS is often used with infants and young children, it is critical to evaluate the effectiveness of motion correction techniques directly with data from these age groups. This study addresses that problem by evaluating motion correction algorithms implemented in HomER2. The efficacy of each technique was compared quantitatively using objective metrics related to the physiological properties of the hemodynamic response. Results showed that targeted PCA (tPCA), Spline, and CBSI retained a higher number of trials. These techniques also performed well in direct head-to-head comparisons with the other approaches using quantitative metrics. The CBSI method corrected many of the artifacts present in our data; however, this approach produced sometimes unstable HRFs. The targeted PCA and Spline methods proved to be the most robust, performing well across all comparison metrics. When compared head-to-head, tPCA consistently outperformed Spline. We conclude, therefore, that tPCA is an effective technique for correcting motion artifacts in fNIRS data from young children.

Keywords: functional near-infrared spectroscopy, motion artifact, child brain imaging, motion correction

Corresponding Author: John P. Spencer, PhD

Evaluating Motion Processing Algorithms for Use with fNIRS Data from Young Children

Functional near-infrared spectroscopy (fNIRS) measures the absorption and scattering of photons as near-infrared light passes through brain tissue, allowing measurement of changes in localized hemodynamic responses in the cortex. It specifically monitors changes in intensity as near-infrared light is passed through tissue from a source to a detector. fNIRS has been widely used to investigate the neural processes that underlie multiple cognitive abilities across development and is becoming a tool of choice when studying challenging populations including infants, young children, and clinical patients who cannot be easily studied with fMRI [1-11]. Despite recent advances in methodological and analytical tools for use with fNIRS data, questions remain regarding the optimal method for removing motion artifacts from the measured signal.

Motion artifacts are often a significant component of the measured fNIRS signal. This is due to the fact that movement can cause transient displacements of the source/detector optodes on the scalp that are reflected in the time-series. The speed and strength of movement as well as the tolerance of the probes to this motion play a role in how these artifacts are reflected in the signal. Motion artifacts are highly variable and often complex. They can be generally classified as spikes, baseline shifts, and low-frequency variations[12] . They take many forms that can appear as isolated, high amplitude events (spikes) or pervasive low-frequency events that are temporally correlated with the measured hemodynamic response and therefore hard to detect and correct for. To estimate the true response, however, it is crucial that motion artifacts are detected and removed.

A variety of methods have been proposed to address this issue. Some include the addition of complementary measurements such as short-separation channels[13, 14] or an accelerometer[15, 16,

Corresponding Author: John P. Spencer, PhD

[17]. These methods provide a direct measure of the artifacts making it possible to regress these artifacts from the measured signal of interest. Alternative approaches include detecting optode fluctuations prior to data collection to prevent unstable and weak connections that would result in motion artifacts[18]. Other approaches take into consideration spatial and/or temporal features of the measured signal and serve as post-processing techniques. Among these approaches are principal component analyses (PCA)[19], Kalman filtering[20], correlation-based signal improvement (CBSI)[21], wavelet filtering[22], spline interpolation[23], autoregressive algorithms[24], and more recently, a kurtosis-based wavelet algorithm[27], empirical mode decomposition (EMD)[25] and an optical model on the influence of optode fluctuation on the fNIRS signal[26].

Several papers have explored the efficacy of different motion correction techniques for fNIRS data[12, 17, 25-33]. The majority of these reports have investigated this problem by adding a simulated hemodynamic response to resting state data. Recently, Chiarelli et al. (2015)[27] introduced a kurtosis-based wavelet algorithm that proved to be more efficient in removing motion artifacts when compared to other techniques in a resting state dataset. Additionally, Gu and colleagues[25] introduced the empirical mode decomposition (EMD) approach which is adaptive and data-driven. This approach performed well when compared to Spline, Wavelet and kurtosis-based wavelet in a resting state dataset by increasing the signal-to-noise ratio and decreasing the mean squared error.

Only two studies have used real, task-based data[12, 30]. Comparison of the techniques has shown that the most effective methods for motion correction are wavelet filtering[12, 28], spline interpolation[28], and targeted PCA (tPCA)[32]. Critically, the complexity of motion artifacts makes it likely that the efficacy of motion correction techniques is data-dependent[12]. Consistent with this, several recent studies have found that wavelet filtering is a promising technique for motion

Corresponding Author: John P. Spencer, PhD

correction; however, the specific type of wavelet filtering that is optimal differs across cohorts and data types. Brigadoi et al. (2014)[12] quantitatively compared 6 motion correction techniques in a sample of adult data measured during a simple cognitive task. They concluded that wavelet filtering showed the most promise as an optimal technique for motion correction. Hu et al. (2015)[30] reported that a combination of wavelet and a moving average yielded the best results in a study of 9- to 12-year-old children.

In the present study, we compared the performance of multiple motion correction techniques as implemented in the HomER2 analysis package[38] using fNIRS data from a cognitive task with young children. The study was unique in two ways. First, our understanding of how motion correction techniques fare when dealing with task-based cognitive data is limited. In the present study, we examined fNIRS data from a study of visual working memory where children had to explicitly compare multiple items from a sample and test array. Second, no previous studies have compared motion correction techniques with fNIRS data from young children. Young children are much more likely to move during data collection, resulting in far noisier data than data from adult participants with motion artifacts distributed throughout the time series. They also routinely engage in jerky movements that can result in more motion epochs and yield artifacts that are faster and of greater amplitude relative to adults. Furthermore, because fNIRS is often used with infants and young children, it is critical to evaluate the effectiveness of motion correction techniques directly with data from these age groups. Thus, we investigated whether the conclusions reached by Brigadoi et al. (2014)[12] extend to data from young children. To address this question, we compared Spline interpolation, PCA, tPCA, Wavelet filtering, and CBSI on data acquired during a working memory paradigm with 3- and 4-year-old children.

Corresponding Author: John P. Spencer, PhD

Note that some adult populations, such as adults with epilepsy, might also produce many motion artifacts. Thus, the issues explored here may be relevant to some adult populations as well. In this context, we note that Selb and colleagues [33] reported that the best approach to minimize the effects of motion artifacts on oscillation fNIRS data from healthy subjects and stroke patients is to correct motion artifacts using a spline interpolation, apply band-pass filtering, and then discard the epochs that were originally identified as containing motion artifacts. We did not evaluate this approach here because data collection with infants, children, and clinical populations often results in quite limited data; consequently, discarding segments of data is not an optimal approach to denoise the optical signal.

Methods

Participants

11 3.5-year-olds (*M*= 3.5 y, *SD*=0.06) and 14 4.5-year-olds (*M*= 4.51 y, *SD*=0.08) participated in the study, after parents provided informed consent. Children were recruited from a participant registry maintained by the Department of Psychology at a Midwestern university in the United States. Parents were sent a letter inviting them to participate and then received a follow-up phone call. All children had normal or corrected-to-normal vision. The study was approved by the university's institutional review board (IRB).

Materials and Procedure

Each participant was seated in front of a 46-inch LCD television that was connected to a PC running E-Prime (Psychology Software Tools, Pittsburgh, PA). The paradigm consisted of a change detection task[34] (figure 1). In this task, participants are presented with a sample array of 1

to 3 colored squares, after which there is a 1s delay, and then a test array appears in which either all the objects match the memory array, or the feature (i.e., color) of one object is changed to a new value. The test display remained on the screen until children provided a verbal response (i.e., 'same' or 'different') that the experimenter entered using a keyboard. After each trial, there was a random inter-trial interval. These intervals consisted of a blank 1 s (50% of trials), 2 s (25% of trials), or 4 s (25% of trials) delay followed by the appearance of a fixation dot. The next trial began once the experimenter pushed a button indicating that the participant was attending to the fixation dot. On average, the total duration of the interval between trials was 12.3 s (*SD* =8.23 s; range varied from 2.23 to 53.32 s).

There were six conditions in the experimental design: children were asked to remember 1, 2, or 3 items (set sizes, SS, 1-3) and the trials either contained a change or did not (same, different). Participants came in for two sessions and completed 24 trials per condition.

fNIRS data

fNIRS data were collected at 50Hz using a TechEn CW6 system with 690nm and 830nm wavelengths. Near-infrared light was delivered via 12 fiber optic cables (sources) to the participant's scalp and detected by 20 fiber optic cables (detectors) spaced into four arrays embedded in a cap. Each array contained three sources and five detectors placed over the frontal, temporal, and parietal cortex bilaterally to tap target regions of interest. Figure 2 shows views of the probe geometry (see Wijeakumar et al., 2015[35] for details). There were a total of 36 channels which formed part of an optimized probe geometry using regions of interest (ROIs) from the fMRI VWM literature [30]. ROIs included included right Superior Intraparietal Sulcus (sIPS), bilateral Intraparietal Sulcus (IPS), bilateral Anterior Intraparietal Sulcus (aIPS), bilateral Ventral

190 Occipital Cortex (VOC), bilateral Dorso-lateral Prefrontal Cortex (DLPFC), left Superior Frontal
191 Gyrus (SFG), bilateral Inferior Frontal Gyrus (IFG), Frontal Eye Fields (FEF), bilateral Middle
192 Frontal Gyrus (MFG), bilateral Occipital (OCC) and bilateral Temporo-parietal Junction (TPJ).
193 To account for variations in head size across participants, source-detector distances were
194 scaled relative to the head circumference using the 10-20 system; thus, the source-detector
195 distance ranged from 25 to 27 mm[35].
196 At the beginning of each session, each participants' head circumference was measured
197 and the appropriate fNIRS cap was selected. Prior to the experimental task, children were fitted
198 with a custom EEG cap that contained grommets to secure the fiber optics to the scalp.
199 Experimenters then cleared out hair that could obstruct the optical signal. Sources and detectors
200 were then fitted into grommets onto the child's head, and secured using an elastic band to limit
201 optode fluctuation as a result of participant movement. The source and detector gains were
202 adjusted to optimize signal quality prior to starting the experimental procedures. Optode
203 positions were recorded in 3-dimensions using a Polhemus Patriot system before the task.
204 The data acquired during this experiment contained a variety of motion artifacts. Figure 3
205 shows an example of the artifacts present in one representative subject's data. Artifacts were
206 generated by the participants' mouth and jaw movements when they gave verbal responses or
207 talked spontaneously as well as by a variety of head and body movements. Figure 4 shows an
208 excerpt of the session video that illustrates some of the movements participants routinely
209 engaged on while completing the task. In particular, the images show how the participant moves
210 his head while changing his line of focus from the display to the experimenter. Note that this
211 period likely included talking with the experimenter. Similarly, the figure also shows how the
212 participant moves back-and-forth while the trial is on. Not all participants had artifacts of the

same type and magnitude, likely because they engaged in slightly different behaviors and had different physical characteristics. However, moving back and forth, changing focus from the display to the experimenter and talking were behaviors that are likely present across all participants. The shape and duration of the artifacts were also variable, although many were fast, high amplitude artifacts. Such individual differences are unavoidable with young children and pose a great challenge when trying to detect and remove motion artifacts using the same method across participants.

Motion correction techniques

Spline interpolation. This method is a channel-by-channel approach based on Scholkmann et al. (2010)[23]. As it is implemented on HomER2[38], this algorithm acts on motion artifacts that have been previously detected; therefore, it is dependent upon having a good motion detection algorithm. Artifacts are modeled using cubic spline interpolation, which is then subtracted from the original time-series to correct for motion artifacts. The time-series is then reconstructed and normalized by shifting the corrected segments by a value given by the combination of the mean value of the segment and the mean value of the previous segment to ensure a continuous signal. For a more detailed description see Scholkmann et al. (2010)[23]. The interpolation depends on a parameter, which determines the degree of the spline function. In this study, the parameter was set to 0.99 to be consistent with previous studies[12, 23, 28].

Principal Component Analysis (PCA). This method applies an orthogonal transformation to decompose the original signal into uncorrelated components based on the amount of variance accounted for by each component. The first components account for the largest proportion of variance and are assumed to represent the motion artifacts as these epochs are characterized by

large changes in amplitude and a high degree of variability. Therefore, removing the first components should correct for motion artifacts[19].

The performance of this technique is highly dependent on both the number of measurements available and the number of components removed. Cooper et al. (2012)[28] suggested that PCA performs optimally when removing 97% of the total variance; thus, we used this value. Following the suggestion of Brigadoi et al. (2014)[12] that 97% was too high, we also performed the correction using 80%. Results for both parameters were very similar; thus, we only include the results for 97% in this report. We also employed a *targeted Principal Component Analysis* (tPCA)[32] which applies a similar PCA filter but only on segments previously identified as motion artifact. Thus, similar to the Spline interpolation method described above, this technique relies on a motion detection algorithm. The corrected motion epochs are then reintroduced to the time series by shifting the corrected segments by a value given by the combination of the mean value of the segment and the mean value of the previous segment to ensure a continuous signal, identical to the procedure employed in the Spline interpolation correction method. This procedure was repeated five times to identify and correct any residual artifacts.

Wavelet filtering. This method is a channel-by-channel approach that follows the one proposed by Molavi and Dumont (2012)[22]. It relies on the differences in amplitude and duration between motion artifacts and the measured signal of interest[22]. As a first step, the signal is expanded using a discrete wavelet transform after which motion artifacts appear as isolated large coefficients. The goal is to remove those coefficients that are not likely to be an outcome of the distribution of wavelet coefficients.

Corresponding Author: John P. Spencer, PhD

The measured signal is assumed to be a sum of the physiological signal of interest and an interference term. The distribution of wavelet coefficients is a mixture of Gaussians[36, 37]. Within this method, the wavelet distribution is assumed to have a single Gaussian probability distribution. Since the hemodynamic signal and motion artifacts differ in timing and amplitude, with the first being a slow and smooth signal, most wavelet coefficients of the signal of interest center around zero while motion artifacts behave like outliers. Therefore, for any given coefficient, if the coefficient exceeds *iqr* times the interquartile range, that coefficient is assumed to not belong in the original signal and must be a reflection of artifacts that should be removed. Iqr was set to 1.0 in this experiment. Outlier terms were removed by setting them to zero preceding the reconstruction of the artifact-free signal by using the inverse discrete wavelet transform.

Correlation-based signal improvement (CBSI). This method is a channel-by-channel approach developed by Cui et al. (2010)[21]. It reduces motion artifacts caused by head movements. The main assumption is that HbO and HbR should be strongly negatively correlated during functional activation and become more positively correlated during motion. Furthermore, the ratio between HbO and HbR is assumed to be the same with and without the presence of motion artifacts. Within this method, the measured signal is assumed to have three components: the true signal of interest, motion-induced noise, and other white noise[21]. Since the white noise component can be easily removed with filters, the purpose then is to compute the true HbO and HbR signal. To do so, two assumptions must be met: first, the correlation between HbO and HbR should be close to -1 and the correlation between the motion artifact and HbO should be close to 0. Solving the following equations should then produce the true signal of interest:

$x_0 = (x - \alpha * y)/2$

Corresponding Author: John P. Spencer, PhD

$y_0 = - (1/ \alpha) * x_0$

with

$\alpha = std(x)/ std(y)$

where std(x) is the standard deviation of x.

Data Processing

The NIRS data were processed using HomER2[38] based in MATLAB (Mathworks, MA USA). Raw optical signals were first converted to optical density. Channels with very low optical density (<80dB; dB=20*LOG10(y), where y is the intensity level measured by the CW6 system) were discarded from the analysis. Incorrect trials were also discarded from further analysis. The mean number of trials included for each participant in each condition was 17.3 (*SD* = 4.8). The mean number of trials per participant and condition was quite high, giving us confidence in the ability to detect differences between the motion processing algorithms.

Selection of motion detection parameters

fNIRS data from young children often has far more motion epochs than data collected from typical adults. Moreover, young children can only perform a handful of trials, making each trial crucially important. Therefore, it is important to employ a set of parameters and a correction technique that recovers as many trials as possible while still decontaminating the data. However, the process of selecting the "right" parameters for a given data set is an ambiguous one. There are no well-defined metrics for setting parameters other than exploring the properties of each data set or using values that other groups have used and exploring how those parameter values affect the data.

Before comparing the motion correction techniques, we explored two different set of motion detection parameters (Table 1). We used the parameters from Brigadoi et al. (2014)[12] as a starting point because this allows for a direct comparison to this previous study. Specifically, motion artifacts were identified in the optical density (OD) time-series using the motion detection algorithm, hmrMotionArtifact. Signal changes with amplitude (AmpThresh) greater than 0.4au and exceeding a threshold of 50 in change of standard deviation (StDevThresh) within 1s were identified as motion artifacts (tMotion). Artifacts were masked for an additional 1s before and after the motion epochs (tMask). Trials were rejected if an artifact appeared 10s after the stimulus onset (enStimRejection: 0-10s). Periods masked as motion artifacts on a given channel were identified on all channels. Note that a channel specific approach, hmrMotionArtifactByChannel, was used for the spline interpolation technique. This algorithm works the same way but on a channel-by-channel basis.

Table 1 | *Motion detection parameters*

	Original Parameters	Relaxed Parameters
tMotion	1	0.3
tMask	1	1
StDevThresh	50	100
AmpThresh	0.4	0.4

This parameter set did a good job identifying a variety of artifacts (fig. 4). However, it resulted in a limited number of trials remaining after motion correction for some motion correction approaches. This might accurately reflect our data: it is possible that there was too much motion in our data set and the excluded trials really should be excluded. Examination of the data set suggested, instead, that the motion detection parameters were too conservative in some cases. For instance, in the lower panel of Figure 4, the first motion artifact is relatively minor, while the second and third artifacts are large.

Corresponding Author: John P. Spencer, PhD

Thus, we took a second look through the data, identifying motion detection parameters that would still do a good job of identifying large motion artifacts in the data, but would let more minor motion artifacts pass through. Note that, although this allows some noise to pass through to the final analysis, this noise trades off with the increase in the number of trials we are averaging over per participant. We relaxed the motion detection parameters (see Table 1) such that signal changes with amplitude greater than 0.4au and exceeding a threshold of 100 in change of standard deviation within 0.3s were identified as motion artifacts. Artifacts were masked for an additional 1s before and after the motion epochs. Thus, in this stage, we are in effect capturing fast, high-amplitude artifacts. The segments identified in yellow in Figure 4 reflect motion detection using the second 'relaxed' set of parameters. As is evident, the second set is most sensitive to fast changes in amplitude. Note, however, that both set of parameters do a good job detecting clear epochs of motion present in the data.

Five processing approaches (PCA, Wavelet, tPCA, Spline, CBSI) were applied to the data after noisy channels were removed. Figure 5 shows the processing stream for all techniques. Four of these techniques (PCA, Wavelet, tPCA, Spline) applied the correction on the OD data. Two of these techniques – tPCA and Spline – did correction based on a first round of motion artifact detection. Here we used the more conservative parameters borrowed from Brigadoi et al.[12] in order to detect – and possibly correct – as much motion as possible. After each correction technique had been applied to the data, motion artifact was detected (assuming motion across all channels) using the 'relaxed' parameters. Trials with motion artifact at this step were rejected. Data were then band-pass filtered (0.016-0.5 Hz) and the concentrations of oxygenated hemoglobin (HbO), deoxygenated hemoglobin (HbR), and total hemoglobin (HbT)

were computed using the modified Beer-Lambert Law[39, 40]. A differential path length (DPF) factor of 6.0 was used for both wavelengths [41].

The fifth correction technique, CBSI, applies the motion correction on concentration changes (see Figure 5). Therefore, the OD data were band-pass filtered and then converted to concentration changes. The correction method was then applied, motion artifact was detected using the 'relaxed' parameters, and trials with motion artifact were rejected. As a final step, the data from the five motion correction techniques were block-averaged to recover the mean hemodynamic response by condition. This yielded six mean measured hemodynamic responses for HbO and HbR for each channel and participant. The performance of these techniques was compared to each other and to uncorrected data.

Quantitative comparison of the approaches

The first step in the quantitative analysis was to identify channels with task-relevant hemodynamic response. The goal was to reduce the number of comparisons and to evaluate the motion correction approaches only on those channels with task-relevant signals. Thus, we compared the concentration of HbO and HbR and included all channels showing a significant difference ($p<0.05$) between these signals within the task-relevant window (0-10 s; see Buss et al., 2014[2]). 34 channels passed this criterion. Next, a block average time series for HbO and HbR was created by averaging data from all six experimental conditions. The central dataset analyzed was from 34 channels and 25 participants contributing two values (HbO and HbR) for each of the metrics described below.

Following Brigadoi et al (2014)[12], we quantitatively compared the efficacy of each correction technique using five metrics. The metrics were defined to provide estimates of how physiologically plausible the recovered mean hemodynamic responses are. The first, the area-

under-the-curve (AUC_{0-2}), encompasses the first two seconds after the onset of the first stimulus array and it is assumed to be composed of artifacts. Therefore, smaller values for this index indicate better performance. The second metric is the AUC_{2-6} that captures the rise and peak of the hemodynamic response specific to our task. Buss et al. (2014)[2] found task-related functional activity between 4-6s after the onset of the first stimulus array in the working memory paradigm used here. Thus, higher values in this time window indicate better performance. Third, we computed the ratio between AUC_{2-6} and AUC_{0-2}. Larger ratio values indicate better performance with low levels of initial noise (AUC_{0-2}) and a strong rise of task-related functional activity (AUC_{2-6}). Fourth, we computed the mean standard deviation of each trial-specific hemodynamic response included in the block average by condition and then averaged across conditions so we end up with one value for this metric for each channel (SubSD). This captures the variability present within subjects. This variability is assumed to be affected by motion artifacts, so higher variability indicates poorer motion correction performance. Finally, we computed the number of trials included after motion correction for each subject and condition. All motion correction techniques were compared to each other quantitatively using ANOVA.

Results

Figure 6 shows the percent of trials recovered after correction by each technique using these parameters. PCA did not recover a substantial number of trials after processing and thus was removed from this stage of the analysis. Figure 7 shows representative examples of a time series pre- and post-correction. The top panel shows the uncorrected OD data while panels B, C, D, and E show the OD data after applying the tPCA, Spline, CBSI and Wavelet techniques, respectively. The figure shows data for three channels (for both wavelengths) with motion epochs color coded by channel. All correction techniques influenced the data by either reducing

391 the amplitude of the artifacts or completely correcting them. The figure also shows that the
392 epochs that remain flagged as artifacts, after correction, are clear motion epochs. Figure 8 shows
393 a representative example of the recovered hemodynamic response. The figure depicts
394 concentration changes across working memory loads (SS1 and SS3) for both HbO and HbR for
395 all motion correction techniques. Overall, all correction techniques effectively remove the
396 motion-induced noise present in the SS1 hemodynamic response. Note that the No Correction
397 plot (top left), shows an increase in both HbO and HbR at SS1 which is inconsistent with
398 functional hemodynamics and could be attributed to motion epochs. Indeed, the figure shows
399 that after motion correction this pattern is no longer present. Note that SS3 evoked a canonical
400 hemodynamic response, with increasing HbO and a decreasing HbR response. Note that CBSI,
401 despite fabricating the hemodynamic response, reduced the HbR response. Similarly, the wavelet
402 algorithm dampened the hemodynamic response.

403 We conducted a mixed factor ANOVA with Technique (CBSI, Wavelet, Spline, tPCA)
404 and Hb (HbO, HbR) as within-subject factors and Age as a between-subject factor on a channel-
405 by-channel basis for the different metrics. For each analysis that showed an effect of Technique
406 (Technique main effect, Technique x Age interaction, or Technique x Hb interaction), we
407 conducted post-hoc comparisons to determine which technique performed quantitatively better
408 along that metric. The number of instances where each technique performed better than its
409 counterparts was tallied. Results are shown in Table 2. Overall, CBSI outperformed the other
410 techniques, with 69 instances where this technique outperformed one of the other techniques.
411 Two other techniques also performed well, namely Spline and tPCA. Note that most of the
412 significant Technique effects were seen on the $AUC_{0\text{-}2}$ and SubSD metrics, while the techniques
413 performed similarly on $AUC_{2\text{-}6}$ and Ratio. Particularly, CBSI outperformed all techniques in the

AUC_{0-2} metric while Spline and tPCA outperformed the other techniques on the SubSD metric. This latter effect is important, showing that Spline and tPCA are effectively reducing the subject-specific variability which is likely influenced by motion artifacts.

Table 2 | *Quantitative analysis summary. Table shows the number of times a technique outperformed its counterparts in channels where there was a significant effect of Technique, Technique by Hb or Technique by Age interaction on each metric*

	Metrics				Total
	AUC02	AUC26	Ratio	SubSD	
CBSI	24	3	3	39	69
WAVELET	6	2	0	13	21
SPLINE	0	4	1	45	50
tPCA	10	1	0	42	53

Figure 9 shows the quantitative metrics across comparisons relative to the data with no motion correction. The top panel of figure 9 shows the mean subject SD for CBSI, Spline, tPCA, and Wavelet relative to No Correction. The techniques performed similarly along this metric and all reduced subject SD relative to No Correction. The bottom panels of Figure 9 show scatter plots of the AUC_{0-2} and AUC_{2-6} values that were computed from the recovered mean hemodynamic response for no motion correction (x axes) and all other techniques (y axes). Results were consistent for both HbO and HbR; thus, results are plotted together. Note that the spread of the data is narrower for the corrected data (y axes), resulting in a cleaner signal for the corrected data.

To ensure all techniques outperformed the data without motion correction, we conducted a mixed factor ANOVA with Technique (No Correction, Correction) and Hb (HbO and HbR) as within-subject factors and Age as a between-subject factor on a channel-by-channel basis for each Technique separately for the different metrics. For each analysis that showed an effect of

Technique, we conducted post-hoc comparisons to determine which technique performed quantitatively better along that metric. Results are shown in Table 3. Consistent with expectations, all the techniques showed a quantitative improvement in the NIRS signal relative to No Correction, although Wavelet showed the weakest performance on this front. As in the previous ANOVA, most significant effects resulted from comparisons of the AUC_{0-2} and the SubSD metrics. For the AUC_{0-2} metric, tPCA substantially outperformed No Correction relative to its counterparts. Similarly, for the SubSD metric, tPCA and Spline outperformed No Correction relative to the other techniques. Note that No Correction outperformed all techniques on the AUC_{2-6} metric. Recall that this metric captures the rise and peak of the hemodynamic response. This suggests that the motion correction techniques are reducing the amplitude of the hemodynamic response as a result of correcting artifacts. Importantly, however, the ratio metric, which is a normalized index of the amplitude relative to the signal at the start of the hemodynamic response window, reveals that tPCA outperformed No Correction in more instances than the other techniques.

Table 3 | *Technique versus no correction. Table shows a summary of the number of times a technique outperformed the no correction method in channels where there was a significant effect of Technique, Technique by Age interaction or technique by Hb interaction on each metric. Numbers in parenthesis indicate the number of times the no correction method outperformed a technique.*

	Techniques (no correction)			
Metrics	CBSI	WAVELET	SPLINE	tPCA
AUC02	20 (0)	24 (0)	27 (5)	44 (0)
AUC26	5 (14)	7 (17)	3 (5)	7 (19)
Ratio	1 (2)	6 (7)	0 (2)	9 (6)
SubSD	57 (0)	39 (26)	87 (0)	90 (0)
Total	83 (16)	76 (50)	117 (12)	150 (25)

Considered together, our results show that CBSI does a good job along some metrics quantitatively, but we note that this technique sometimes yields inconsistent corrected hemodynamic responses. tPCA and Spline, on the other hand, do a good job quantitatively across the board and yield robust measured hemodynamic responses. Thus, as a last analysis step, we explored how these two approaches fared against each other.

A mixed factor ANOVA with technique (Spline, tPCA) and Hb (HbO and HbR) as within-subject factors and Age as a between-subject factor was computed on a channel-by-channel basis for each of the metrics. The number of instances where each technique performed better than its counterpart in channels with a significant effect of Technique were tallied. Overall, tPCA outperformed Spline in 35 versus 13 cases across all metrics. Thus, tPCA appears to be the most effective motion correction method for our data set.

Note that an additional set of analyses following the procedure from Buss et al. (2014)[2] was implemented to explore whether removing outliers would influence how these techniques perform. Outlier trials were removed that contained amplitudes that were more than 3.5 standard deviations above or below a participant's mean in each condition for 18 consecutive time-samples. A technique X outlier removal ANOVA was computed for all the metrics. Given that some of these techniques rely on the variability present in the time series, we hypothesized that removing outlier observations from the data would improve how the techniques performed. This was not the case; removing outliers did not have a significant effect on the performance of the techniques for any of the quantitative metrics (p>.05).

Discussion

Given the prevalence of motion artifacts, several recent papers have evaluated the efficacy of different motion correction techniques for fNIRS data. These comparisons have

478 mostly relied on simulated data; less is known about how these techniques work on empirical
479 data from cognitive tasks. Brigadoi et al. (2014)[12] showed that Wavelet outperformed the other
480 motion techniques in a data set from adult participants, while Hu et al. (2015)[30] showed that a
481 combination of wavelet filtering and a moving average outperformed other techniques on a data
482 set from older children (mean age = 9.9 years). In the present study, we used a comparable
483 approach to examine which techniques are most effective with data from young children. This is
484 an important contribution given that data from young children often has more, and potentially
485 different, motion artifacts. Moreover, discarding trials due to motion is less viable given that
486 participants can only complete a handful of trials. Note that the present investigation may also
487 provide useful information for researchers using fNIRS to study brain activity in aging adults or
488 patient populations (i.e., epileptic or Alzheimer's patients). Like young children, these
489 participants may generate a higher quantity of motion artifacts and may also generate different
490 kinds of motion artifacts. Selb at al.[33] reported that the best way to limit the effect of motion
491 artifacts in oscillation data from stroke patients is to discard the contaminated epochs. This
492 approach, is not optimal given how frequent these artifacts can be present in these population.
493 Thus, continuous development of correction techniques and the investigating its effects with
494 real-task based data, remains an important topic of study.

495 In their report, Hu et al.[30] classified motion artifacts info four different types. Those types
496 include fast spikes (within 1s), peaks with a standard deviation of 100 from the mean with a
497 duration of 1 to 5s, gentle slopes between 5 and 30s that deviated 300 from the mean, and a slow
498 baseline shift longer than 30s. In the present study, motion artifacts consisted primarily of type 1
499 from Hu et al., that is, fast spikes (0.3-1s).

Our results suggest that CBSI was effective at correcting for motion artifacts for some metrics, although a qualitative look at how CBSI affected the resultant hemodynamic response across conditions raised concerns that this approach might be producing unstable hemodynamic responses. tPCA and Spline performed more robustly, outperforming the other motion correction techniques both in the number of trials recovered and across multiple quantitative metrics of interest. Note that both of these techniques rely on a first pass of motion artifact detection and we used conservative detection parameters from Brigadoi et al.[12] for this initial pass through the data. This has the advantage of detecting multiple types of motion epochs and attempting to correct them. Then, we used relaxed motion detection parameters in the second pass to exclude primarily fast spikes and allow more data to pass through to the block average for each participant. This approach seemed quite effective. Although both approaches fared well, in a head-to-head comparison, tPCA performed quantitatively better. Thus, we conclude that tPCA is the most effective motion correction technique with our data.

Another advantage of tPCA is that it targets specific epochs where the artifacts are present[32]. Given that motion artifacts are often distributed throughout a data collection session, this means that fewer trials are likely to be lost due to motion. This is particularly important in cases where there is a high quantity of artifacts and a small number of trials. Consistent with this, the PCA algorithm – which does not target motion epochs, but rather requires that an artifact be presented in multiple channels to be identified as a principal component – eliminated too many trials to make it viable for our dataset.

The Spline technique performed well in the quantitative analysis but interestingly, it did not fully correct as many artifacts as other techniques (see figure 7), even though it does reduce the amplitude of these epochs. This could explain why it performed similarly to the No

Correction method on the Ratio metric. Previous studies have reported that Spline can yield inconsistent results across studies [12, 23, 28, 30, 42]. This technique works by generating a cubic spline function based on previously detected artifacts and then removing this function from the signal. The inconsistency might arise because artifacts can be highly variable; thus, using umbrella parameters (i.e., the same parameters across participants) could result in the interpolation function fitting some artifacts but not others.

One concern with the motion correction approaches is that they appear to be dampening the resultant amplitude of the hemodynamic response. For instance, after correction, the signal amplitude in Figure 9 is narrow, particularly for Wavelet. Recall that in this manuscript we calculated an average measured hemodynamic response across conditions to reduce the number of comparisons. This could be having a dampening effect in the measured response. However, this effect could also suggest that when many artifacts are present, there is a risk of over-correcting, that is, removing important variance from the hemodynamic response of interest. This is particularly plausible in data from young children where artifacts are distributed throughout the time series, including within the response of interest. In the present report, the amplitudes of the resultant hemodynamic response when plotted by condition were around 0.2 μM. hemodynamic response amplitudes from our previous study[2] were in the same range (0.2 - 0.5 μM). Thus, it appears that overcorrection is not a major concern here. That said, it is important to tailor the motion correction parameters to the properties of each data set to ensure that overcorrection does not occur.

Our results also provide insights into why some techniques perform better than others with data from young children. For instance, techniques that do not rely on any motion detection algorithm and assume that an artifact should be present on multiple channels, such as PCA,

546 performed poorly because this assumption was not met in our data; consequently, these
547 approaches eliminated too many trials. On the contrary, techniques relying on motion detection
548 performed better because, after detection and then correction, more trials are kept, thus
549 increasing the signal to noise ratio of the data. Furthermore, our data suggest that tPCA
550 performed better than Spline because Spline removes the signal when an artifact is identified. If
551 many motion artifacts are identified, as in our dataset, this method removes potentially useful
552 signal. By contrast, tPCA removes only some of the variance, potentially retaining a portion of
553 the signal of interest even if many artifacts are identified. These results highlight the importance
554 of not only selecting the right parameters when processing fNIRS data but also sheds light on
555 why some techniques outperform others with highly contaminated data.

556 Great strides have been made in finding reliable motion correction techniques for fNIRS
557 data. Our study has contributed to this body of work by evaluating different techniques head-to-
558 head with data from young children from a cognitive task, and considering multiple motion
559 detection parameter settings. Of course, new motion processing approaches are always in
560 development; thus, future work will be needed to continually re-evaluate new approaches such as
561 a recent kurtosis-based wavelet filtering approach[27], empirical mode decomposition (EMD) [25], an
562 optical model on the influence of optode fluctuation on the fNIRS signal[26] as well as the
563 autoregressive algorithm developed by Barker et al. (2013)[24]. We note that the autoregressive
564 algorithm was not included in our analysis because this approach uses deconvolution techniques
565 rather than the block average approach evaluated here.

566 Note that Umeyama's approach to detect optode fluctuations prior to starting data
567 collection provides a great advancement in our understanding of how some artifacts are
568 generated[18], and could potentially help reduce the quantity of artifacts. We suspect, however, that

this approach may have limited application with young children given that it adds an extra step to data collection which might result in the participant not completing the task. Future work should investigate Yamada's optical model[26] to correct for these placement faults in data from children.

Although our results provide evidence that tPCA is a promising choice for correcting motion artifacts in fNIRS data, it is necessary to consider some details about our design. In this experiment, we used a variable inter-trial-interval (mean 12.3s, min 2.3s), mostly driven by the child being ready and paying attention to continue on to the next trial. This, of course, means that the hemodynamic response of interest, recovered by block average, is different for short ITI vs long ITI trials. However, this added between-trials variability is present for all techniques; thus, we do not think this concern undermines our conclusions. Furthermore, the differential path length factor used in the study was the default parameter in HomER2, 6.0 for both wavelenghts, and was not corrected for age. Note that recent work by Li et al.[43], used the same parameter (6.0) in a comparable sample (3-5 year-olds). Previous work suggests that a DPF of 4.8-5.13, depending on the wavelength, should be used when estimating concentration changes in frontal-frontotemporal data from children[44]. However, anatomical differences across individuals may also play a role in regard to this calculation[44]. While we acknowledge this parameter is important to accurately model concentration changes, we used a parameter previously used in the literature[43] and kept it consistent across techniques thus we do not think this undermines out conclusions. Future work should explore if this has an effect in our ability to investigate the efficacy of motion correction techniques.

Conclusion

Correcting motion artifacts that contaminate the signal of interest is a critical step when processing fNIRS data. To estimate the true hemodynamic response, it is crucial that these

592 artifacts are detected and removed. Our results showed that tPCA, Spline, Wavelet and CBSI
593 outperformed PCA in terms of retaining a higher number of trials. CBSI, Spline and tPCA also
594 performed well in direct head-to-head comparisons with the other approaches using a set of
595 quantitative metrics. The CBSI method corrected many of the artifacts present in our data;
596 however, this approach produced sometimes unstable corrected hemodynamic responses. The
597 targeted PCA and Spline methods, on the other hand, proved to be the most robust, performing
598 well across all comparison metrics. When compared head-to-head, tPCA consistently
599 outperformed Spline. This is consistent with what Yücel et al. (2014)[32] reported when comparing
600 tPCA, Spline, and Wavelet in a data set where a synthetic hemodynamic response was
601 introduced to a raw NIRS signal. Thus, we conclude that tPCA is a promising choice for
602 correcting motion artifacts in fNIRS data from young children as well as data sets with a high
603 number of motion artifacts.
604
605

Corresponding Author: John P. Spencer, PhD

606 Disclosures

607 The authors have no conflict of interest.

608

609

610

611

612

613

614

615

616

617

618

619

620

621

622

623

624

625

626

627

628

Corresponding Author: John P. Spencer, PhD

Acknowledgments

We would like to thank David Boas for his assistance in understanding and evaluating the motion processing algorithms. This work was supported by OPP1119427 from the Bill & Melinda Gates Foundation awarded to JPS and by the NSF GRFP under Grant No. 1048957 awarded to LDR. Finally, we thank the parents and children who participated in the study, and the undergraduate research assistants in the SPAM lab.

Corresponding Author: John P. Spencer, PhD

669 References
670
671 1. Boas, D. A., Elwell, C. E., Ferrari, M., & Taga, G. (2014). Twenty years of functional near-
672 infrared spectroscopy: introduction for the special issue. *NeuroImage*, *85 Pt 1*, 1–5.
673 http://doi.org/10.1016/j.neuroimage.2013.11.033
674 2. Buss, A.T., Fox, N., Boas, D.A., Spencer, J.P., (2014). Probing the early development of
675 visual working memory capacity with functional near-infrared spectroscopy.
676 *NeuroImage*. *85*, 314-315. http://doi.org/10.1016/j.neuroimage.2013.05.034.
677 3. Farroni, T., Chiarelli, A.M., Lloyd-Fox, S., Massaccesi, S., Merla, A., Di Gangi, V.,
678 Mattarello, T., Faraguna, D., Johnson, M.H. (2013). Infant cortex responds to other humans
679 from shortly after birth. *Sci. Rep.* 3, 2851.
680 4. Fabiani, M., Gordon, B.A., Maclin, E.L., Pearson, M., Brumback, C.R., Low, K.A., McAuley,
681 E., Sutton, B.P., Kramer, A.F., Gratton, G. (2014). Neurovascular coupling in normal aging:
682 a combined optical, ERP and fMRI study. *NeuroImage* 1, 592–607.
683 5. Fallgatter, A.J., Roesler, M., Sitzmann, A., Heidrich, A.,Mueller, T.J., Strik, W.K. (1997).
684 Loss of functional hemispheric asymmetry in Alzheimer's dementia assessed with
685 nearinfrared spectroscopy. *Cogn. Brain Res*. 6, 67–72.
686 6. Gallagher, A., Thériault, M., Maclin, E., Low, K., Gratton, G., Fabiani, M., Lassonde, M.
687 (2007). Near-infrared spectroscopy as an alternative to theWada test for language mapping
688 in children, adults and special populations. *Epileptic Disord*. 9,
689 241–255

690 7. Grossmann, T., Johnson, M.H., Lloyd-Fox, S., Blasi, A., Deligianni, F., Elwell, C., Csibra, G.
691 (2008). Early cortical specialization for face-to-face communication in human infants. *Proc.
692 R. Soc. B Biol. Sci*. 275, 2803–2811.

Corresponding Author: John P. Spencer, PhD

8. Lloyd-Fox, S., Blasi, A., Elwell, C.E. (2010). Illuminating the developing brain: the past, present and future of functional near infrared spectroscopy. *Neurosci. Biobehav. Rev*. 34, 269–284.

9. Mahmoudzadeh, M., Dehaene-Lambertz, G., Fournier, M., Kongolo, G., Goudjil, S., Dubois, J., Grebe, R., Wallois, F. (2013). Syllabic discrimination in premature human infants prior to complete formation of cortical layers. *Proc. Natl. Acad. Sci*. 110, 4846–4851.

10. Roche-Labarbe, N., Zaaimi, B., Berquin, P., Nehlig, A., Grebe, R., Wallois, F. (2008). NIRS measured oxy-and deoxyhemoglobin changes associated with EEG spike-and-wave discharges in children. *Epilepsia* 49, 1871–1880.

11. Zhu, H., Fan, Y., Guo, H., Huang, D., & He, S. (2014). Reduced interhemispheric functional connectivity of children with autism spectrum disorder: evidence from functional near infrared spectroscopy studies. *Biomedical optics express*, *5*(4), 1262-1274.

12. Brigadoi, S., Ceccherini, L., Cutini, S., Scarpa, F., Scatturin, P., Selb, J., … Cooper, R. J. (2014). Motion artifacts in functional near-infrared spectroscopy: A comparison of motion correction techniques applied to real cognitive data. *NeuroImage*, *85*, 181–191. http://doi.org/10.1016/j.neuroimage.2013.04.082

13. Robertson, F.C., Douglas, T.S., Meintjes, E.M. (2010). Motion artifact removal for functional near infrared spectroscopy: a comparison of methods. IEEE Trans. Biomed. Eng. 57 (6), 1377–1387.

14. Gagnon, L., Yücel, M. A., Boas, D. A., & Cooper, R. J. (2014). Further improvement in reducing superficial contamination in NIRS using double short separation measurements. *NeuroImage*, *85 Pt 1*, 127–35. http://doi.org/10.1016/j.neuroimage.2013.01.073

Corresponding Author: John P. Spencer, PhD

15. Blasi, A., Phillips, D., Lloyd-Fox, S., Koh, P.H., Elwell, C.E. (2010). Automatic detection of motion artifacts in infant functional optical topography studies. *Oxygen Transp. Tissue* 31, 279–284.

16. Virtanen, J., Noponen, T., Kotilahti, K., Virtanen, J., & Ilmoniemi, R. (2011) Accelerometer-based method for correcting signal baseline changes caused by motion artifacts in medical near-infrared spectroscopy. *J. Biomed. Opt*. 16(8), 087005.

17. Metz, A. J., Wolf, M., Achermann, P., & Scholkmann, F. (2015). A new approach for automatic removal of movement artifacts in near-infrared spectroscopy time series by means of acceleration data. *Algorithms*, *8*(4), 1052–1075. https://doi.org/10.3390/a8041052

18. Umeyama, S., & Yamada, T. (2013). Detection of an unstable and/or a weak probe contact in a multichannel functional near-infrared spectroscopy measurement. *Journal of Biomedical Optics*, *18*(4), 47003. https://doi.org/10.1117/1.JBO.18.4.047003

19. Zhang, Y., Brooks, D.H., Franceschini, M.A., Boas, D.A. (2005). Eigenvector-based spatial filtering for reduction of physiological interference in diffuse optical imaging. J. Biomed. Opt. 10 (1), 11014.

20. Izzetoglu, M., Chitrapu, P., Bunce, S., Onaral, B. (2010). Motion artifact cancellation in NIR spectroscopy using discrete Kalman filtering. Biomed. Eng. Online 9–16.

21. Cui, X., Bray, S., Reiss, A.L., 2010. Functional near infrared spectroscopy (NIRS) signal improvement based on negative correlation between oxygenated and deoxygenated hemoglobin dynamics. NeuroImage 49 (4), 3039–3046.

22. Molavi, B., Dumont, G.A., 2012. Wavelet-based motion artifact removal for functional

near-infrared spectroscopy. Physiol. Meas. 33 (2), 259–270.

23. Scholkmann, F., Spichtig, S., Muehlemann, T., Wolf, M. (2010). How to detect and reduce movement artifacts in near-infrared imaging using moving standard deviation and spline interpolation. Physiol. Meas. 31 (5), 649–662.

24. Barker, J. W., Aarabi, A., & Huppert, T. J. (2013). Autoregressive model based algorithm for correcting motion and serially correlated errors in fNIRS. *Biomedical Optics Express*, *4*(8), 1366–79. http://doi.org/10.1364/BOE.4.001366

25. Gu, Y., Han, J., Liang, Z., Yan, J., Li, Z., & Li, X. (2016). Empirical mode decomposition-based motion artifact correction method for functional near-infrared spectroscopy. *Journal of Biomedical Optics*, *21*(1), 15002. https://doi.org/10.1117/1.JBO.21.1.015002

26. Yamada, T., Umeyama, S., & Ohashi, M. (2015). Removal of motion artifacts originating from optode fluctuations during functional near-infrared spectroscopy measurements. *Biomedical Optics Express*, *6*(12), 4632. https://doi.org/10.1364/BOE.6.004632

27. Chiarelli A. M., Maclin E. L., Fabiani M., Gratton G., (2015). A kurtosis-based wavelet algorithm for motion artifact correction of fNIRS data. *Neuroimage*, 112, 128–137 10.1016/j.neuroimage.2015.02.057

28. Cooper, R.J., Selb, J., Gagnon, L., Phillip, D., Schytz, H.W., Iversen, H.K., Ashina, M., Boas, D.A., (2012). A systematic comparison of motion artifact correction techniques for functional near-infrared spectroscopy. *Front. Neurosci*. 6, 147.

29. Tak, S., & Ye, J. C. (2014). Statistical analysis of fNIRS data: a comprehensive review. *NeuroImage*, *85*, 72-91.

Corresponding Author: John P. Spencer, PhD

30. Hu, X.S., Arredondo, M.M., Gomba, M., Confer, N., DaSilva, A.F., Johnson, T.D., Shalinsky, M. & Kovelman, I. (2015). Comparison of motion correction techniques applied to functional near-infrared spectroscopy data from children. *Journal of Biomedical Optics*, *20*(12), 126003-126003.

31. Selb J, Yücel MA, Phillip D, Schytz, H., Iversen, H., Vangel, M., & Boas DA. (2015). Effect of motion artifacts and their correction on near-infrared spectroscopy oscillation data: a study in healthy subjects and stroke patients. *J. Biomed. Opt*. 0001;20(5):056011.

32. Yücel, M. a, Selb, J., Cooper, R. J., & Boas, D. a. (2014). Targeted principle component analysis: A new motion artifact correction approach for near-infrared spectroscopy. *Journal of Innovative Optical Health Sciences*, *07*(02), 1350066. http://doi.org/10.1142/S1793545813500661.

33. Selb, J., Yücel, M. A., Phillip, D., Schytz, H. W., Iversen, H. K., Vangel, M., Ashina, M., Boas, D. A. (2015). Effect of motion artifacts and their correction on near-infrared spectroscopy oscillation data: a study in healthy subjects and stroke patients. *Journal of Biomedical Optics*, *20*(5), 56011. https://doi.org/10.1117/1.JBO.20.5.056011

34. Simmering Vanessa R. (2012). The development of visual working memory capacity during early childhood. *Journal of experimental child psychology*, 111(4):695–707

35. Wijeakumar, S., Spencer, J. P., Bohache, K., Boas, D. a., & Magnotta, V. A. (2015). Validating a new methodology for optical probe design and image registration in fNIRS studies. *NeuroImage*, *106*, 86–100. http://doi.org/10.1016/j.neuroimage.2014.11.022

Corresponding Author: John P. Spencer, PhD

778 36. Antoniadis, A., Bigot, J., & Sapatinas, T. (2001). Wavelet estimators in nonparametric
779 regression: a comparative simulation study. *Stat. Softw.* 83 1–83
780 37. Chipman, H. A., Kolaczyk, E. D., & McCulloch, R. E. (1997). Adaptive Bayesian Wavelet
781 Shrinkage. *Journal of the American Statistical Association*.
782 38. Huppert, T.J., Diamond, S.G., Franceschini, M.A., Boas, D.A. (2009). HomER: a review of
783 time-series analysis methods for near-infrared spectroscopy of the brain. Appl. Opt. 48 (10),
784 D280–D298. www.nmr.mgh.harvard.edu/PMI/resources/homer2
785 39. Cope, M., Delpy, D.T., 1988. System for long-term measurement of cerebral blood and
786 tissue oxygenation on newborn infants by near infra-red transillumination. *Med.*
787 *Biol. Eng. Comput*. 26 (3), 289–294
788 40. Delpy, D.T., Cope, M., van der Zee, P., Arridge, S., Wray, S., Wyatt, J., 1988. Estimation of
789 optical pathlength through tissue from direct time of flight measurement. *Phys.*
790 *Med. Biol.* 33 (12), 1433–1442.
791 41. Strangman, G., Franceschini, M. A., & Boas, D. A. (2003). Factors affecting the accuracy of
792 near-infrared spectroscopy concentration calculations for focal changes in oxygenation
793 parameters. NeuroImage, 18(4), 865–879. https://doi.org/10.1016/S1053-8119(03)00021-
794 1

795 42. Vinette, S. A., Dunn, J. F., Slone, E., & Federico, P. (2015). Artifact reduction in long-term
796 monitoring of cerebral hemodynamics using near-infrared
797 Spectroscopy. *Neurophotonics*, *2*(2), 025004-025004.

798 43. Li, Y., Grabell, A. S., Wakschlag, L. S., Huppert, T. J., & Perlman, S. B. (2017). The neural

substrates of cognitive flexibility are related to individual differences in preschool irritability: A fNIRS investigation. Developmental Cognitive Neuroscience, 25, 138–144. https://doi.org/10.1016/j.dcn.2016.07.002

44. Scholkmann, F., & Wolf, M. (2013). General equation for the differential pathlength factor of the frontal human head depending on wavelength and age. *Journal of Biomedical Optics*, *18*(10), 105004. https://doi.org/10.1117/1.JBO.18.10.105004

Figure Captions

Figure 1 | Change detection task. Sequence of events during a trial. Each trial began with an auditory prompt saying, “Let's look for color changes!” along with a fixation circle on the left or right side of the screen that preceded where the target stimuli appeared. The experimenter initiated the trial when the child was ready. The sample array then appeared on the screen for 2 s, followed by a blank interval of 1 s. The test array was then presented until the child verbally responded “same” or “different”. The experimenter entered the child's response on a keyboard.

Figure 2 | Probe geometry. Panel A shows two views of the probe geometry. Red circles depict sources and blue circles depict detectors while yellow lines represent the channels. Figure was created using AtlasviewerGUI (HOMER2, Massachusetts General Hospital/Harvard Medical School, MA, U.S.A.). Panel B shows a schematic of the left side view of the probe.

Figure 3 | **Motion Artifacts.** Example motion artifacts (highlighted in pink) present during a segment of the time series for one channel for one participant. The red line shows the 690 nm wavelength while the 830 nm wavelength is shown in blue. Vertical lines depict the onset of a trial (i.e., timepoint 0). The figure shows the raw time series, before any motion correction is applied and before band pass filtering.

Figure 4 | Examples of motion artifacts (highlighted in pink for the parameters used in stage 1 and yellow for the revised parameters) present during a segment of the time series for one channel for one participant. The red line shows the 690 nm wavelength while the 830 nm wavelength is shown in blue. Vertical lines depict the onset of a trial (i.e., time point 0). The bottom panel shows an excerpt of this participant’s behavior while completing the task.

Figure 5 | Processing stream for all techniques. Processing steps for all techniques are represented by a colored arrow: green for CBSI, blue for PCA, purple for Wavelet, red for tPCA, orange for Spline and gray for no correction. Note that tPCA and Spline require motion to be detected before applying the correction.

Figure 6 | Figure shows the percent of trials recovered using each motion processing technique.

Corresponding Author: John P. Spencer, PhD

839

840 **Figure 7 | Pre- and post-motion correction.** The figure depicts example channel before and
841 after each motion processing technique is applied. The time series plotted is optical density data.
842 The solid line shows the 690 nm wavelength while the 830 nm wavelength is depicted by the
843 dotted lines. The shaded areas reflect motion artifacts, color coded to reflect each channel.
844 Vertical lines depict the onset of a trial (i.e., time point 0).
845

846 **Figure 8 | Hemodynamic responses examples.** Figure shows an example of the recovered
847 hemodynamic response as the working memory load increases for a channel in the left frontal
848 cortex for each of the motion correction technique. Solid lines represent HbO^2 and dotted lines
849 represent HbR.
850

851 **Figure 9 |** Results for the comparison analysis. Top Panel shows the mean standard deviation
852 averaged across subjects. Error bars depict the standard error of the mean. The bottom panel
853 shows the scatter plots for the $AUC_{0\text{-}2}$ and $AUC_{2\text{-}6}$ metric for both HbO (shown in red circles)
854 and HbR (shown in blue triangles), no motion correction on the X axes vs CBSI, Spline, tPCA
855 and Wavelet on the Y axes.
856
857

Corresponding Author: John P. Spencer, PhD

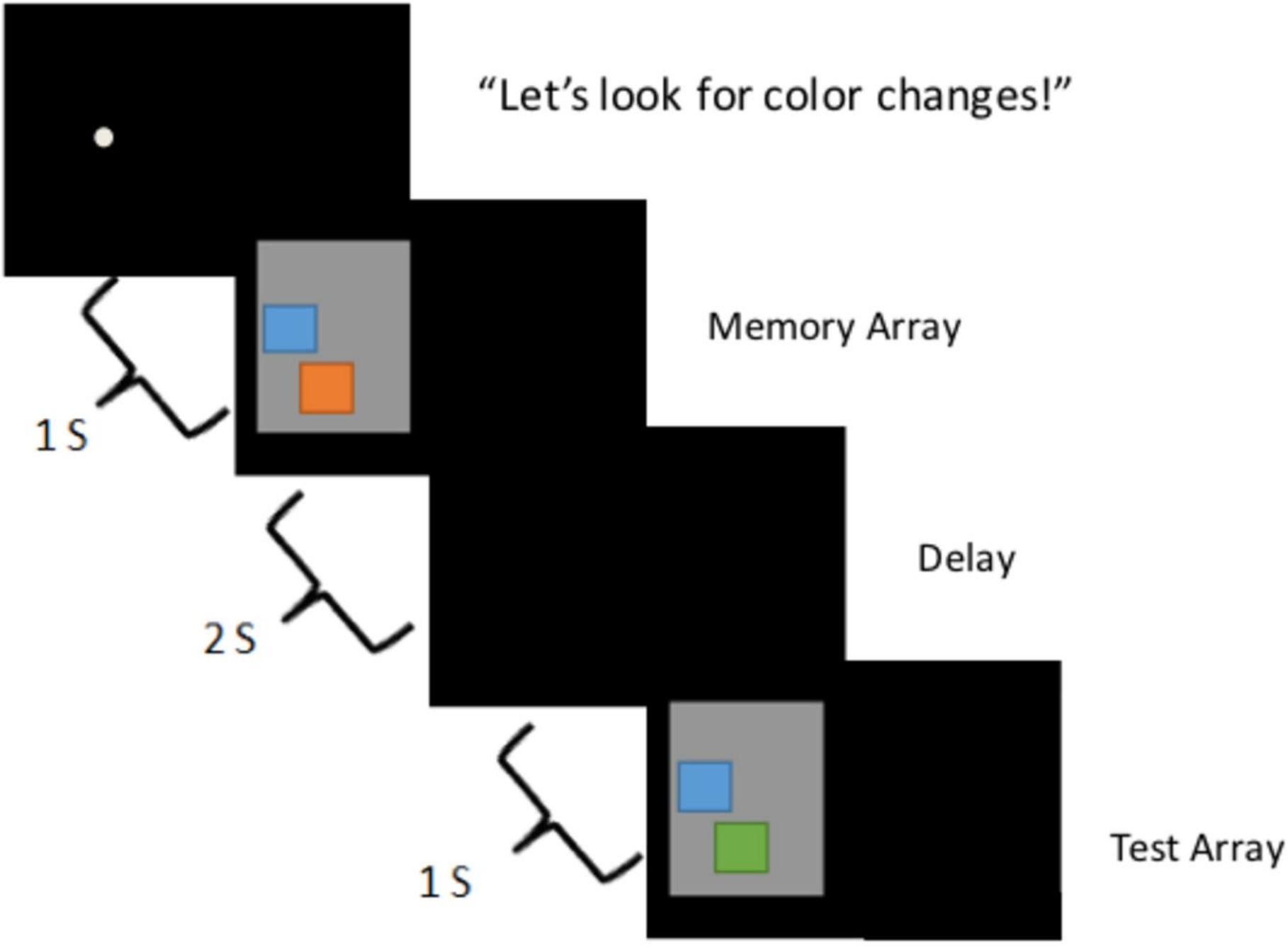
"Let's look for color changes!"
Memory Array
1 S
Delay
2 S
1 S
Test Array

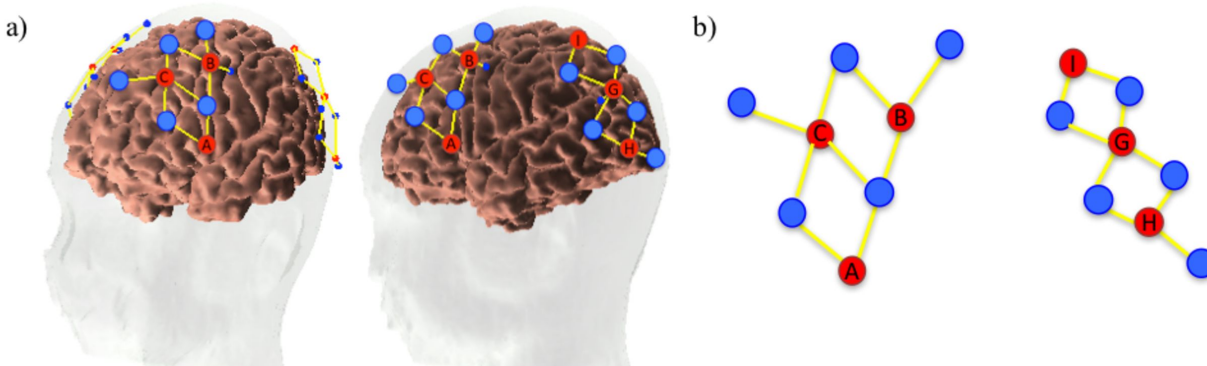
a)
C
B
A
C
B
A
I
G
H
b)
C
B
A
I
G
H

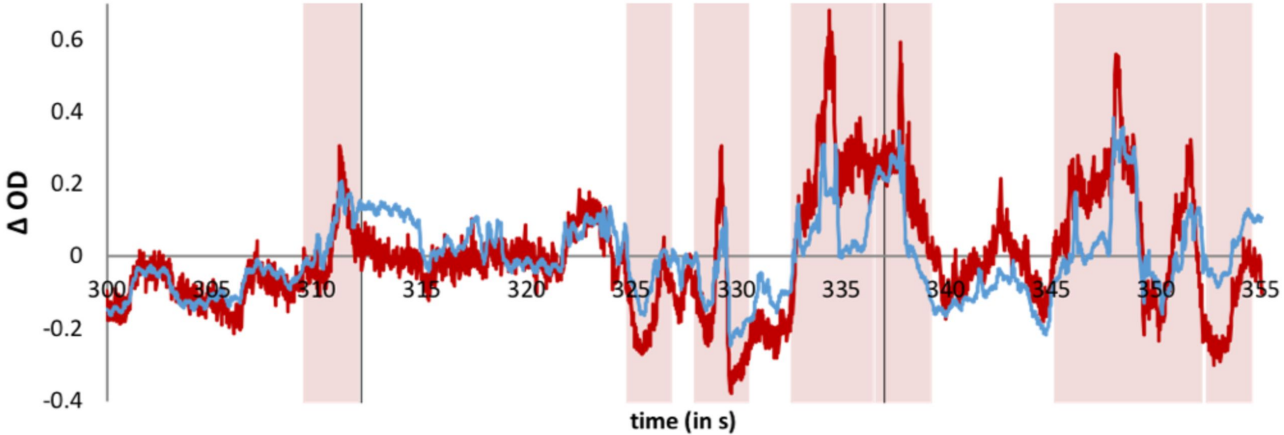
0.6
0.4
0.2
0
-0.2
-0.4
Δ OD
300
305
310
315
320
325
330
335
340
345
350
355
time (in s)

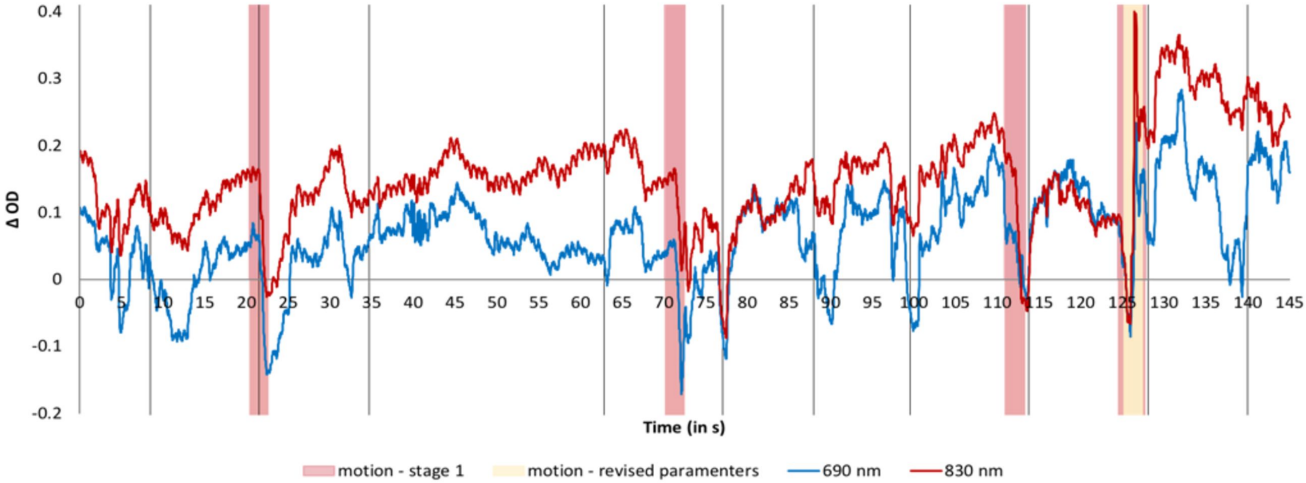
0.4
0.3
0.2
0.1
0
-0.1
-0.2
Δ OD
0 5 10 15 20 25 30 35 40 45 50 55 60 65 70 75 80 85 90 95 100 105 110 115 120 125 130 135 140 145
Time (in s)
motion - stage 1
motion - revised paramenters
690 nm
830 nm

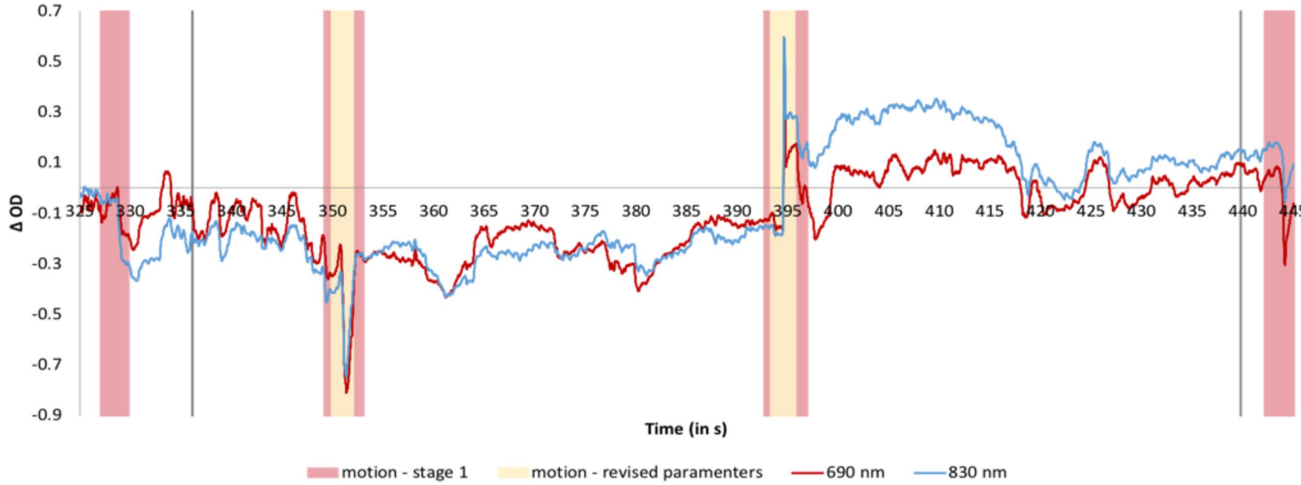
0.7
0.5
0.3
0.1
-0.1
-0.3
-0.5
-0.7
-0.9
Δ OD
325 330 335 340 345 350 355 360 365 370 375 380 385 390 395 400 405 410 415 420 425 430 435 440 445
Time (in s)
motion - stage 1
motion - revised paramenters
690 nm
830 nm

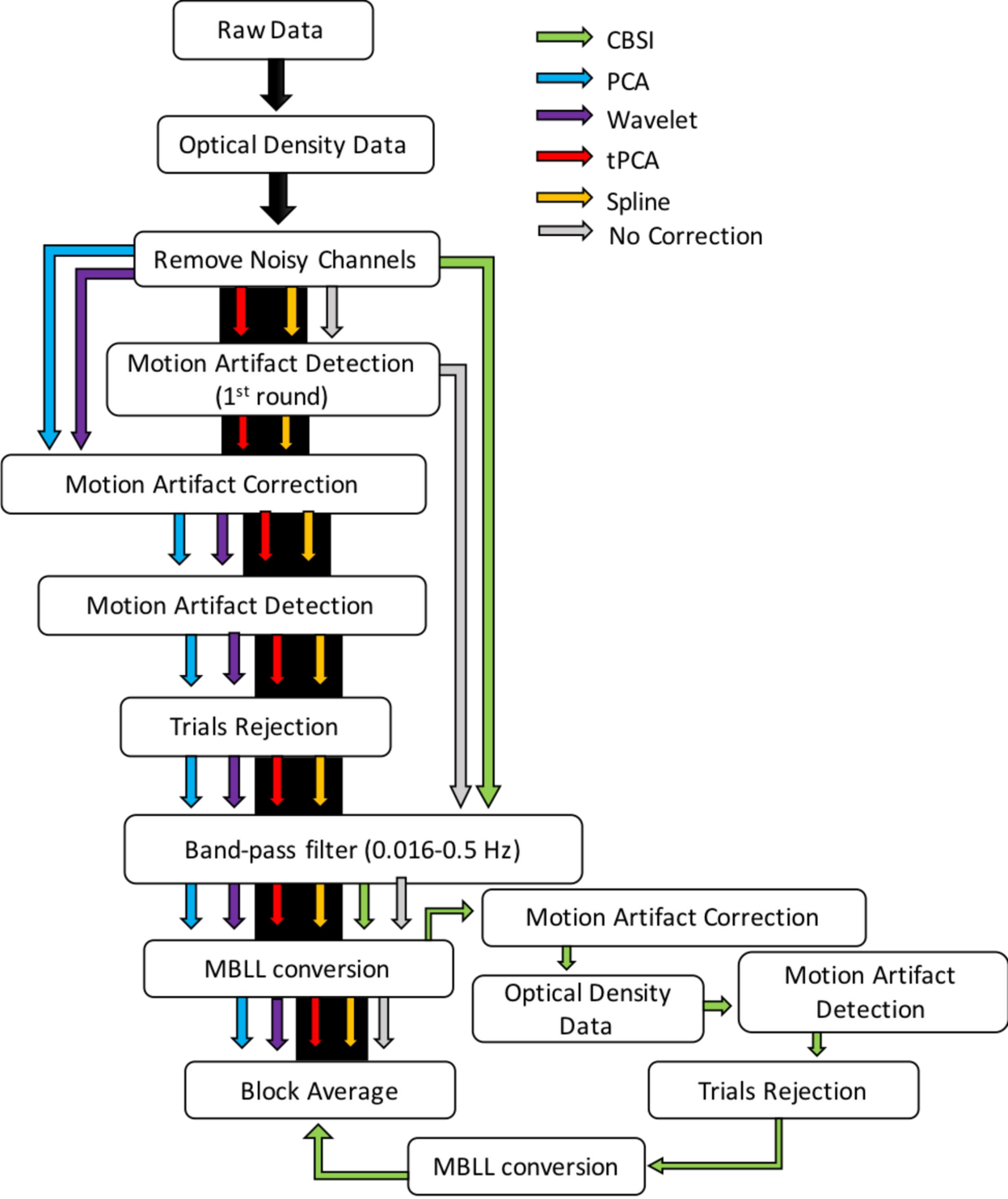
Raw Data
Optical Density Data
Remove Noisy Channels
Motion Artifact Detection (1st round)
Motion Artifact Correction
Motion Artifact Detection
Trials Rejection
Band-pass filter (0.016-0.5 Hz)
MBLL conversion
Block Average
Motion Artifact Correction
Optical Density Data
Motion Artifact Detection
Trials Rejection
MBLL conversion
CBSI
PCA
Wavelet
tPCA
Spline
No Correction

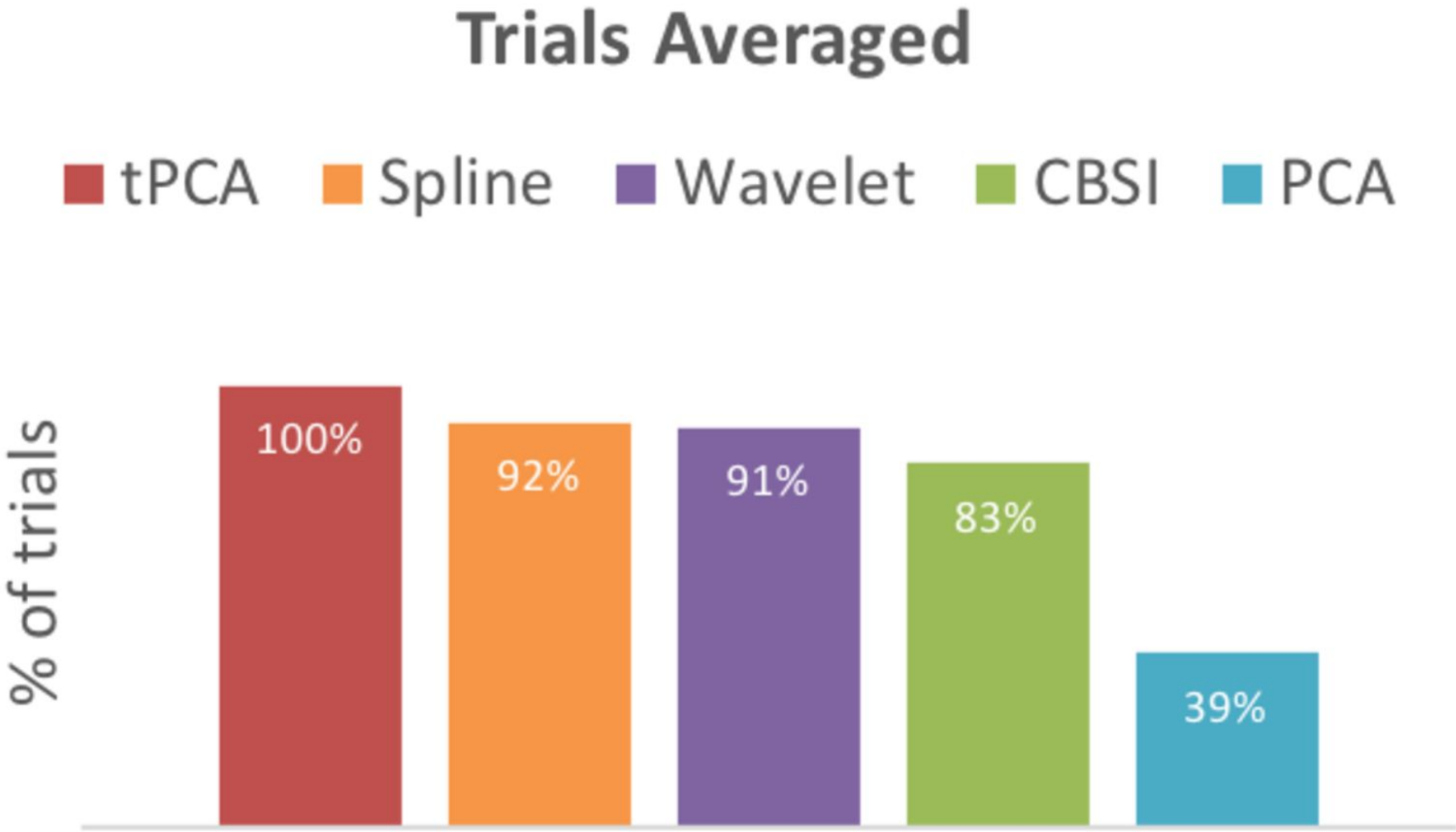
Trials Averaged
tPCA
Spline
Wavelet
CBSI
PCA
% of trials
100%
92%
91%
83%
39%

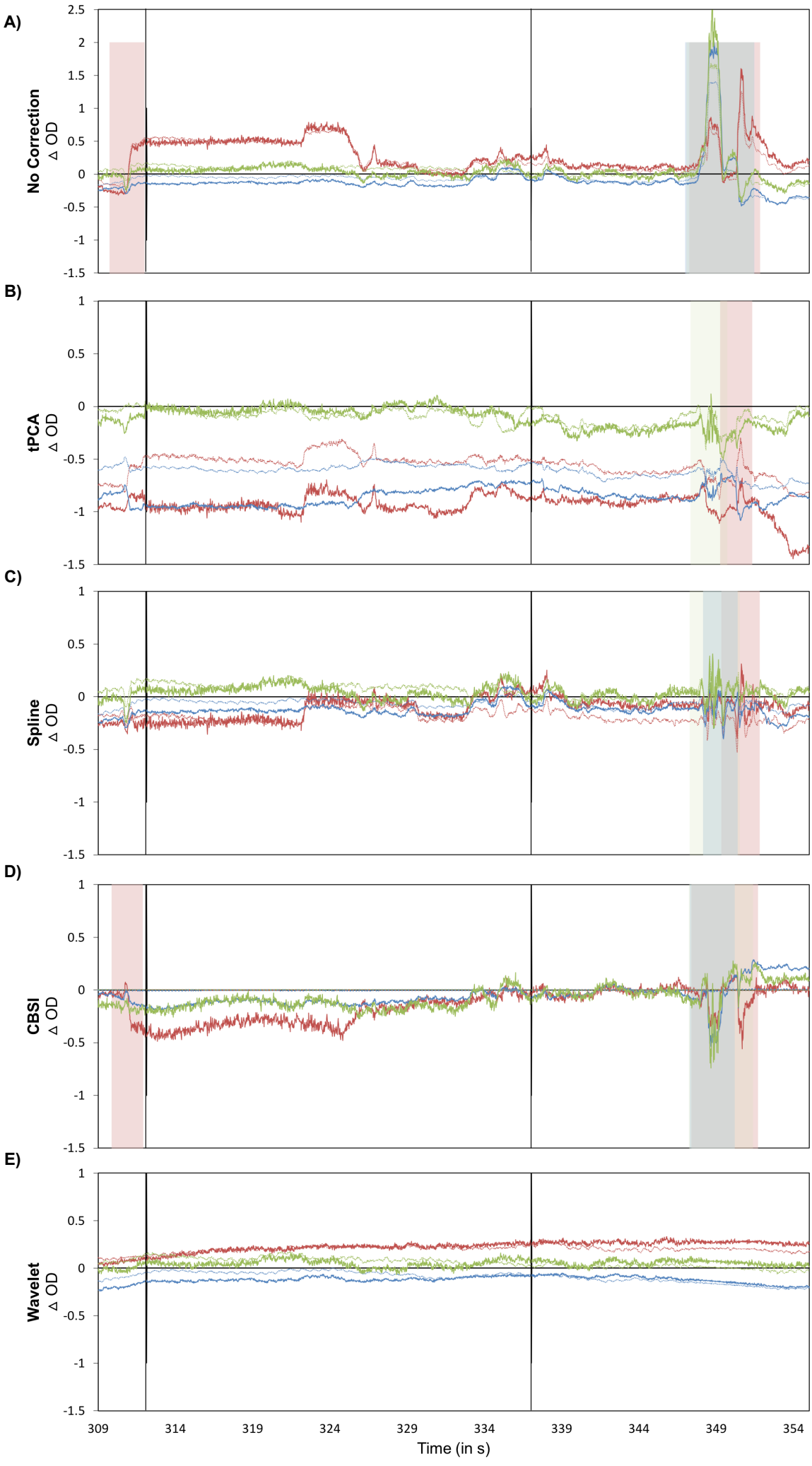
A)
No Correction
Δ OD
B)
tPCA
Δ OD
C)
Spline
Δ OD
D)
CBSI
Δ OD
E)
Wavelet
Δ OD
Time (in s)

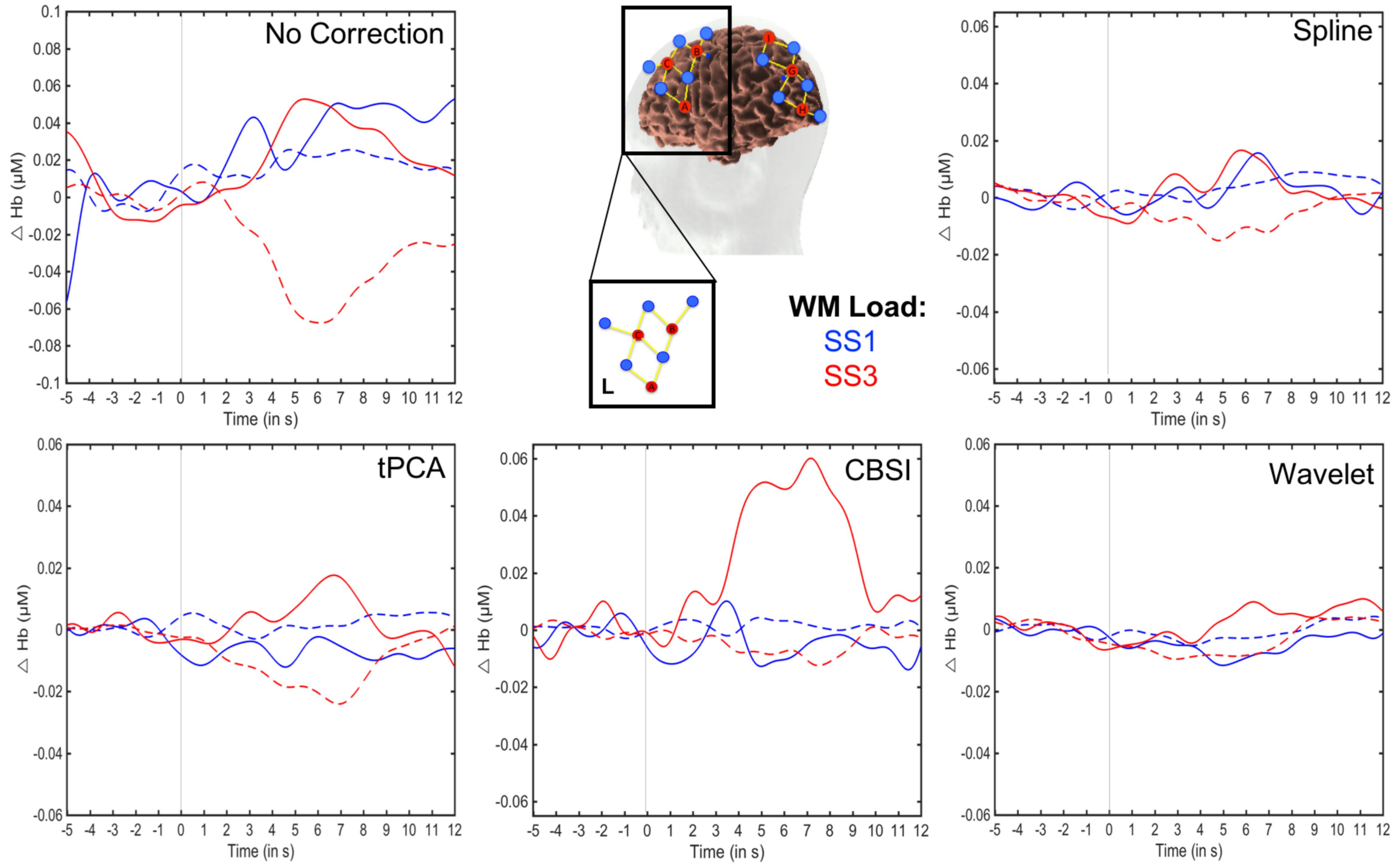
No Correction
Spline
tPCA
CBSI
Wavelet
△ Hb (μM)
Time (in s)
WM Load:
SS1
SS3
L
A
B
C
G
H
I

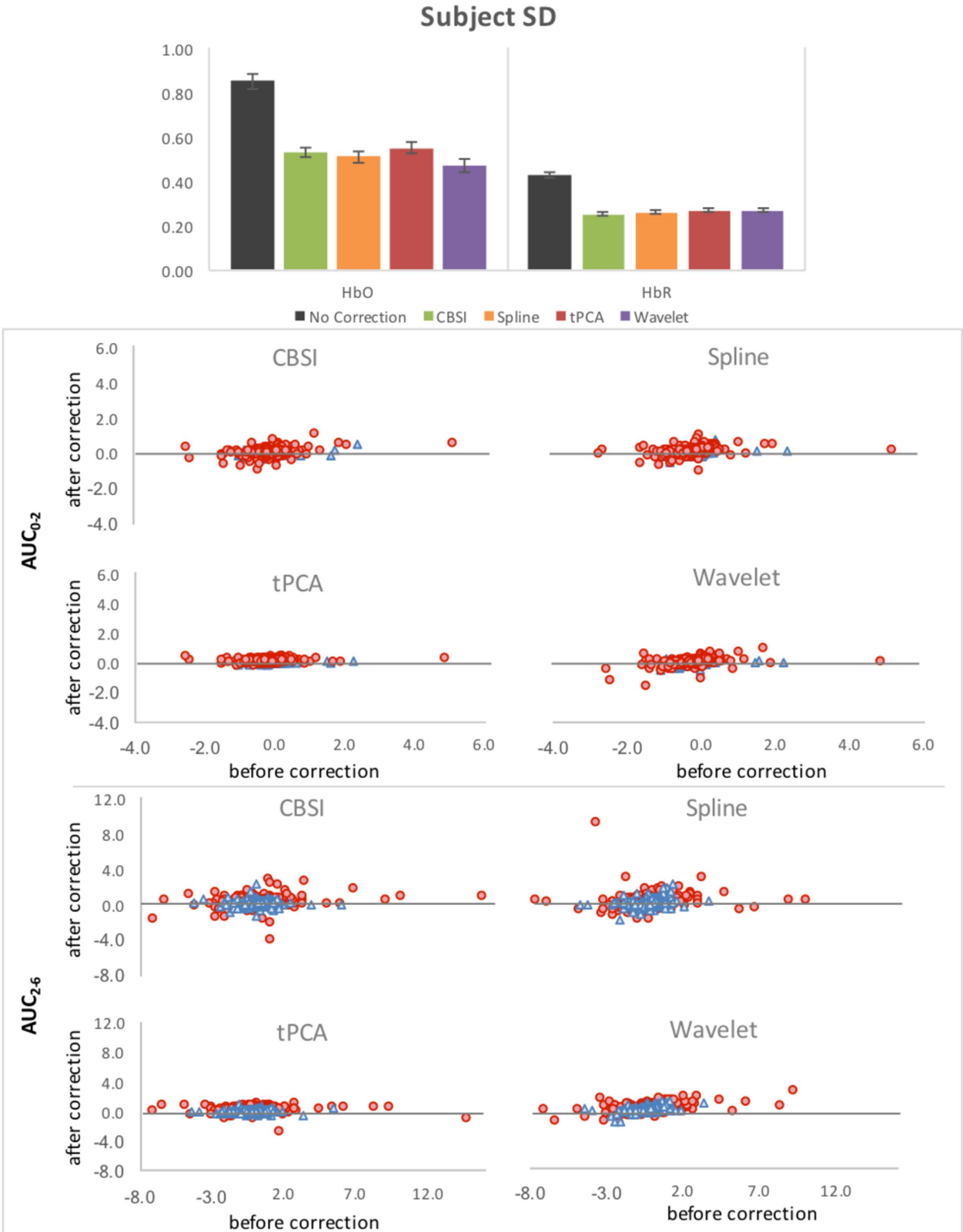
Subject SD
1.00
0.80
0.60
0.40
0.20
0.00
HbO
HbR
No Correction
CBSI
Spline
tPCA
Wavelet
AUC0-2
AUC2-6
after correction
before correction
CBSI
Spline
tPCA
Wavelet
6.0
4.0
2.0
0.0
-2.0
-4.0
12.0
8.0
-8.0
-3.0
2.0
7.0